

Anderson localization transition in a robust \mathcal{PT} -symmetric phase of a generalized Aubry–André model

Sebastian Schiffer,* Xia-Ji Liu, Hui Hu, and Jia Wang†

Centre for Quantum Technology Theory, Swinburne University of Technology, Melbourne 3122, Australia

(Dated: October 20, 2020)

We study a generalized Aubry–André model that obeys \mathcal{PT} -symmetry. We observe a robust \mathcal{PT} -symmetric phase with respect to system size and disorder strength, where all eigenvalues are real despite the Hamiltonian being non-unitary. This robust \mathcal{PT} -symmetric phase can support an Anderson localization transition, giving a rich phase diagram as a result of the interplay between disorder and \mathcal{PT} -symmetry. Our model provides a perfect platform to study disorder-driven localization phenomena in a \mathcal{PT} -symmetric system.

Introduction.—Out-of-equilibrium open quantum systems are ubiquitous, where energy, particles, and information can transfer to or from the surrounding environment. In some limits, non-Hermitian Hamiltonians can well describe the quantum behavior of these systems [1–9]. The presence of complex eigenvalues of non-Hermitian Hamiltonians is a direct consequence of the non-preservation of probability due to loss and gain. However, non-Hermitian Hamiltonians that exhibit parity-time (\mathcal{PT}) symmetry can still possess a purely real spectrum, indicating the loss and gain are coherently balanced [10]. \mathcal{PT} -symmetry refers to the invariance of Hamiltonian under a combined parity (\mathcal{P}) and time-reversal (\mathcal{T}) transformation, but not necessarily with \mathcal{P} and \mathcal{T} separately. Furthermore, a spontaneous \mathcal{PT} -symmetry breaking may occur when the degree of non-Hermiticity is large enough, where eigenvalues that come in complex conjugate pairs appear. We usually name the real (complex) spectral phase as a \mathcal{PT} -symmetric (-broken) phase.

\mathcal{PT} -symmetry became an active research area since the original work by Bender and Boettcher [10]. Applications of \mathcal{PT} -symmetry have been found in various physics areas, ranging from quantum field theories and mathematical physics [11–14] to solid-state physics [15] and optics [16–21]. It has recently attracted intense interest due to the rapid progress in atomic, molecular, and optical (AMO) experiments, where engineered loss and gain is accessible in a controllable manner [21–30]. In particular, the real-to-complex spectral transition (\mathcal{PT} transition) has been observed both in classical [31] and quantum systems [32].

Another theoretical concept that has also gained a lot of attention recently thanks to experimental developments in photonic crystals [33–37] and ultracold atoms [38, 39] is Anderson localization [40]. Anderson localization refers to the absence of a particle’s diffusion induced by disorder. In a one-dimensional (1D) lattice model, an on-site cosine modulation incommensurate with the underlying lattice can be regarded as a highly corre-

lated disorder, in a loose qualitative sense, and hence sometimes called quasi-disorder. Aubry and André (AA) showed that a 1D tight-binding model with a quasi-disorder has a self-dual symmetry and manifests as a localization phase transition for all eigenstates at a critical modulation strength [41]. This seminal work stimulated extensive theoretical and experimental investigations in various generalized AA models [42–51].

Localization transition can also occur in a non-Hermitian Hamiltonian system, such as non-Hermitian extensions of AA model [52–54] and the Hatano-Nelson model with asymmetric hopping amplitudes [55–58]. A very recent study gives an interesting topological interpretation for the existence of the localization transition in Hatano-Nelson model [59]. However, whether an Anderson localization transition can exist in a \mathcal{PT} -symmetric Hamiltonian remains elusive. On the one hand, an exponential localization state induced by disorder requires a very large system size and can only be stable in the \mathcal{PT} -symmetric phase. On the other hand, an uncorrelated disorder usually does not respect \mathcal{PT} -symmetry, making the \mathcal{PT} -symmetric phase disappear for an arbitrarily weak disorder strength [60, 61]. Even in a few studies that use an engineered \mathcal{PT} -symmetric disorder, the \mathcal{PT} -symmetric phase is still generally very fragile in the sense that it exists only for an exponentially small non-Hermiticity parameter in the large system size limit [15, 62–64]. Interestingly, the \mathcal{PT} -symmetric phase becomes robust if an asymmetric hopping is introduced, implying Anderson localization might exist [62, 65–67].

We study a generalized AA model with commensurate modulation in both on-site potentials and asymmetric imaginary hopping terms in this work. The phase diagrams in Fig. 1 show our main results: (1) a robust \mathcal{PT} -symmetric phase exists for large system sizes and arbitrary disorder strength; (2) a disorder-driven localization transition occurs within the \mathcal{PT} -symmetric phase on a quarter circle arc $\sqrt{t^2 + \gamma_0^2} = V_0$ as phase boundary; (3) along this phase boundary and $t = 0, \gamma_0 \geq V_0$, the system shows critical behavior; (4) in the \mathcal{PT} -broken phase the eigen wavefunctions are extensive.

Generalized AA Model.—The Hamiltonian of the one-dimensional (1D) generalized AA model we consider here

* sschiffer@swin.edu.au

† jiawang@swin.edu.au

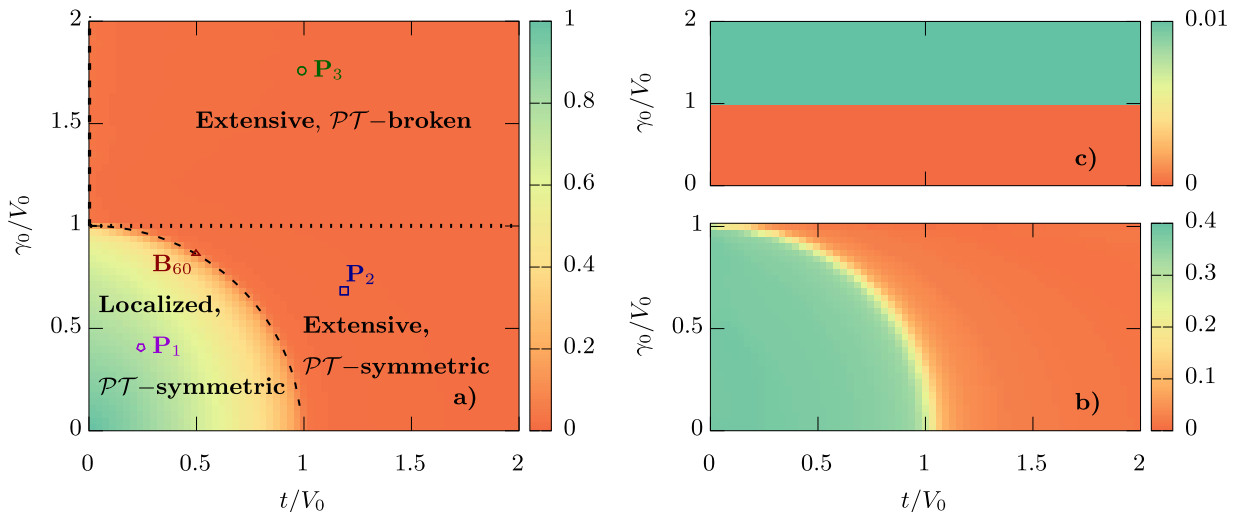


FIG. 1: Phase diagrams of the system for $N = 233$. a) and b) show $\langle \text{MIPR} \rangle$ and gap statistics $\langle r \rangle$ respectively, both of which identify a localized phase within the quarter circle $\sqrt{t^2 + \gamma_0^2} \leq V_0$. c) shows $\langle I_{\mathcal{PT}} \rangle$ that reveals the robust \mathcal{PT} -symmetric phase exist for $\gamma_0 < 1$ for arbitrary t/V_0 . The localization-transition and \mathcal{PT} -transition boundaries are also indicated in a) by the thin dashed curve and the dotted line respectively. A thick dashed line illustrates the “special ray” $\{t = 0, \gamma > 1\}$ detailed in the main text. We also mark several specific points P_1 , P_2 , P_3 and B_{60} in different phase regimes, which correspond to $\{t/V_0, \gamma_0/V_0\} \approx \{0.24, 0.42\}$, $\{1.2, 0.69\}$, $\{1.0, 1.74\}$ and $\{\cos(60^\circ), \sin(60^\circ)\}$. We exemplify properties of different phases on these points as detailed in the main text.

is given by

$$\hat{H} = \sum_{j=1}^N \left[t_j \hat{c}_{j+1}^\dagger \hat{c}_j + t_{j+1} \hat{c}_j^\dagger \hat{c}_{j+1} + V_j \hat{c}_j^\dagger \hat{c}_j \right], \quad (1)$$

where \hat{c}_j^\dagger (c_j) is the creation (annihilation) operator at site j , and the subindex j should be understood as $j \pmod{N}$. The on-site modulation is given by $V_j = 2V_0 \cos(2\pi\beta j + \varphi)$, and the hopping is complex and asymmetric: $t_j = t + i\gamma_0 \sin(2\pi\beta j + \varphi) \neq t_{j+1}^*$. Here V_0 is the quasi-disorder strength, and γ_0 controls the non-Hermiticity. We also choose $\beta = M/N$, where M and N are two adjacent Fibonacci numbers, which are mutually prime. When $\gamma_0 = 0$, the model Hamiltonian reduces back to the traditional AA model.

We analytically prove that this Hamiltonian is \mathcal{PT} -symmetric for a set of modulation phase factors $\varphi_{\mathcal{PT}} \equiv m\pi/N$, where m are odd (integer) numbers if N is even (odd) [68]. Surprisingly, we numerically observe that, under some conditions, the system’s spectrum remains (up to the numerical accuracy) all real or complex-conjugate-paired for *any arbitrary* φ . We test the violation of \mathcal{PT} -symmetry of our Hamiltonian by defining a measure that vanishes if all eigenenergies E_k are either real or complex-conjugate-paired:

$$S_{\mathcal{PT}} = \sum_k^N |\Im(E_k)| \prod_{m \neq k}^N [1 - \delta(E_k, E_m)] + \frac{1}{2} \sum_k^N \sum_{m \neq k}^N \delta(E_k, E_m) |\Im(E_k) + \Im(E_m)|, \quad (2)$$

where $\delta(E_k, E_m) = 1$ if the difference of the real parts is small enough i.e. $|\Re(E_k) - \Re(E_m)| < \epsilon_{\text{tol}}$, and 0 otherwise. We choose a tolerance $\epsilon_{\text{tol}} = 10^{-4}V_0$ for the numerical implementation. Here, we use \Re (\Im) to denote the real (imaginary) part. Figure 2 shows some typical behavior of the maximum of $S_{\mathcal{PT}}/I_{\mathcal{PT}}$ over φ as a function of N ($I_{\mathcal{PT}}$ is defined in Eq. (3) to characterise whether the spectrum is purely real, and merely serves as a normalization factor here). Our numerical result shows that $S_{\mathcal{PT}}$ are always vanishingly small for even chains (i.e. N is even). For long enough ($N > 89$) odd chains, $S_{\mathcal{PT}}$ is also as small as the numerical precision except at the

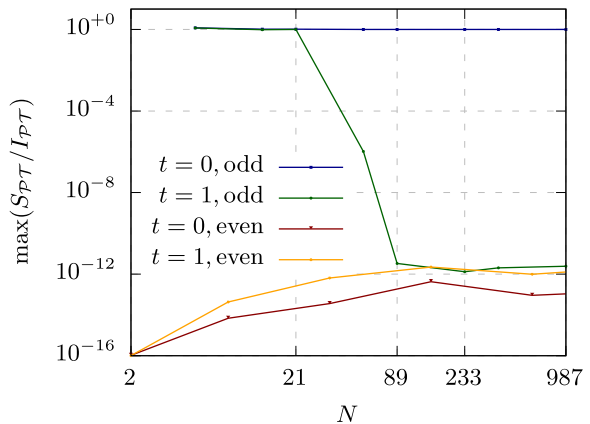


FIG. 2: Maximum violation of the \mathcal{PT} -symmetry $S_{\mathcal{PT}}/I_{\mathcal{PT}}$ for even and odd chains at $\gamma_0 = 2$, $t = 0$ and $t = 1$.

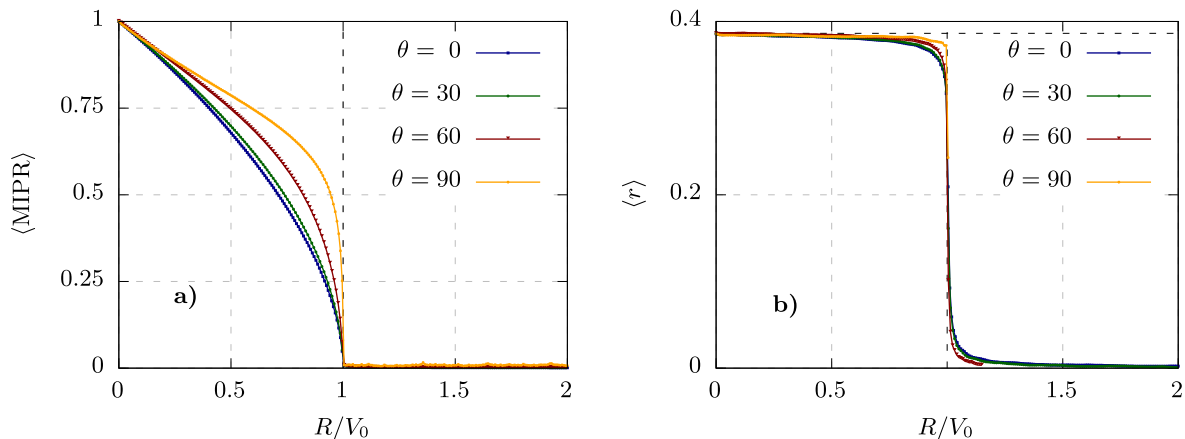


FIG. 3: $\langle \text{MIPR} \rangle$ and $\langle r \rangle$ as a function of $R = \sqrt{t^2 + \gamma_0^2}$. a) shows the $\langle \text{MIPR} \rangle$ at several different $\theta = \tan^{-1}(\gamma_0/t)$, indicating the localization transition occurs at $R = V_0$ for all θ . b) shows the gap statistics $\langle r \rangle \approx 0.38$, the Poisson distribution value, in the strong disorder limit $t/V_0 \rightarrow 0$, and a rapid decay at the localization transition boundary.

ray $\{t = 0, \gamma_0 > V_0\}$ in the $t/V_0 - \gamma_0/V_0$ parameter space, which is called “special ray” for convenience hereafter. We remark here that, for analyzing the disorder-driven localization transition, it is vital that the spectrum remains purely real or complex-conjugate-paired for arbitrary φ since it allows us to average over the phase factor φ to emulate disorder realization. Hereafter, unless specified otherwise, we always average observables over φ and denote the average as $\langle \cdot \rangle$, except at the special ray, where we only calculate for $\varphi = \varphi_{\mathcal{PT}}$.

\mathcal{PT} -broken phase.—For \mathcal{PT} -symmetric systems, the \mathcal{PT} -symmetry might be spontaneously broken, if the degree of non-Hermiticity is large enough [69]. In our system, we explore the parameter space to find both symmetry-broken and -unbroken regions. As the appearance of complex conjugate pairs in the spectrum of a \mathcal{PT} -symmetric system indicates the broken phase, we define a \mathcal{PT} -symmetry indicator as sum over the absolute values of the imaginary parts of the spectrum

$$I_{\mathcal{PT}} = \sum_k |\Im(E_k)|, \quad (3)$$

which vanishes if the spectrum is purely real. We observe that $\langle I_{\mathcal{PT}} \rangle$ abruptly changes from finite to vanishingly small at the vicinity of $\gamma_0 = V_0$ irrespective of the value of t/V_0 , marking the boundary between \mathcal{PT} -symmetric and broken phase as depicted in Fig. 1(c). The fact that a \mathcal{PT} -transition occurs at $\gamma_0 = V_0$ for arbitrary t/V_0 implies the \mathcal{PT} -symmetric phase in our system is robust against strong disorder. We have also confirmed that this \mathcal{PT} -phase diagram is essentially unchanged for larger N , indicating the robustness against system size. The robustness of the \mathcal{PT} -symmetric phase in our system is in stark contrast to most previous studies, where the \mathcal{PT} -symmetric phase becomes exponentially fragile in the presence of disorder.

Localization.—Next, we investigate the system for its localization behavior. A widely used measure for local-

ization is the inverse participation ratio (IPR) [70]. For a normalized wavefunction $\psi(j)$ of an hermitian Hamiltonian, the IPR is defined as the summation of the probability over all the sites $\sum_j p(j)^2 \equiv \sum_j |\psi(j)|^4$. In the case of non-hermitian Hamiltonians, the left and right eigenvectors can be orthonormalised in the sense that $\sum_j \psi_m^L(j)^* \psi_k^R(j) = \delta_{mk}$, where $p_k^L(j) = \psi_k^L(j)^* \psi_k^R(j)$ plays a similar role as probability at site j . Thus we define the IPR measure as [71]

$$\text{IPR}_{\text{LR}}(E_k) = \left[\frac{\left(\sum_j |\psi_k^L(j) \psi_k^R(j)| \right)^2}{\sum_j |\psi_k^L(j) \psi_k^R(j)|^2} \right]^{-1}, \quad (4)$$

which varies from being $\mathcal{O}(1/N)$ for eigenfunctions smeared uniformly over all sites to $\mathcal{O}(1)$ for those localized near a specific site. Therefore, the IPR can serve as an indicator for the localization transition. Averaging the IPR over all eigenfunctions and all quasi-disorder realizations gives the mean inverse participation ratio $\langle \text{MIPR} \rangle = \langle \sum_k \text{IPR}_{\text{LR}}(E_k) / N \rangle$ [68]. Figure 3 (a) shows the $\langle \text{MIPR} \rangle$ as a function of $R = \sqrt{t^2 + V_0^2}$ for various $\theta = \text{atan}(\gamma_0/t) \in [0^\circ, 90^\circ]$. These calculations are carried out for $N = 1597$, where the numeric is well converged. The $\langle \text{MIPR} \rangle$ monotonically decreases from one to zero in the regime $R/V_0 \in [0, 1]$ and slower for larger θ . The $\langle \text{MIPR} \rangle$ also essentially remains zero in the regime $R > V_0$ for any θ . In the $t/V_0 - \gamma_0/V_0$ parameter space, R/V_0 can be recognised as the distance to the origin, and θ as the angle to the t -axis. Therefore, the localization boundary is located at the quarter circle arc $\sqrt{t^2 + \gamma_0^2} = V_0$, which is also illustrated in the phase diagram in Fig. 1 a).

We also perform an energy gap statistic analysis to diagnose the localization transition. As the energies can be complex in the \mathcal{PT} -broken regime, we restrict this analysis to the region $\gamma_0 \leq V_0$, where the averaged level

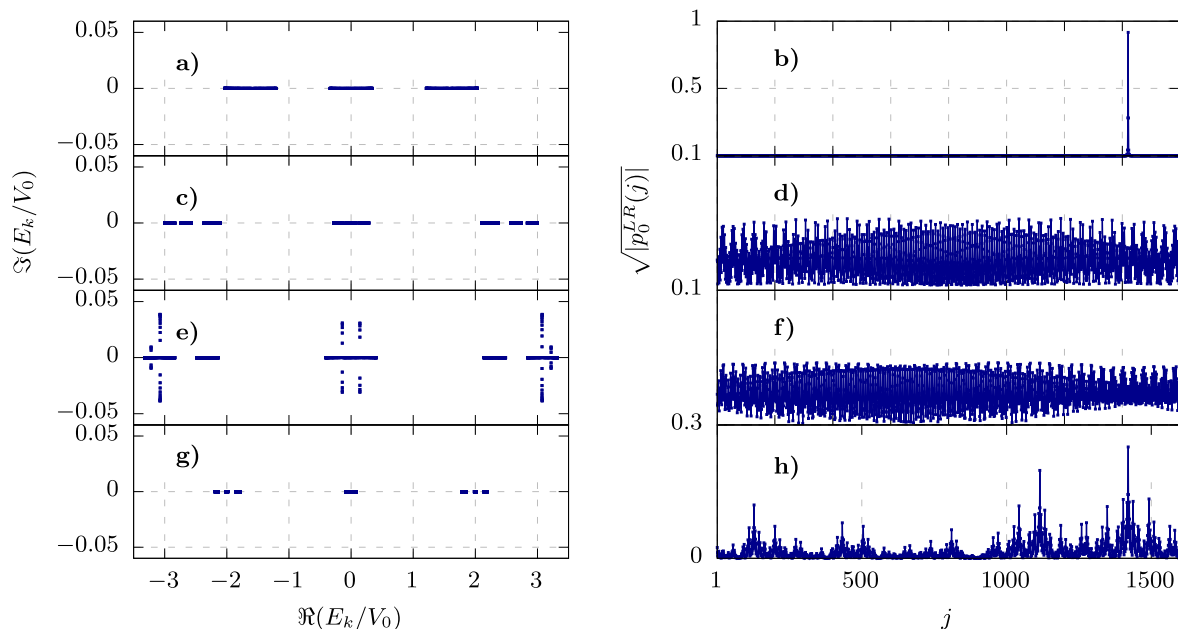


FIG. 4: Energy spectra $\Im(E_n)$ as a function of $\Re(E_n)$ and $\sqrt{|p_0^{LR}(j)|}$ of the state with $E_0 \approx 0$ for $N = 1597$ for the different sets of parameters marked in Fig. a). The spectra are shown in a) c) e) and g) and the wavefunction are shown in b) d) f) h) for P_1 , P_2 , P_3 and B_{60} respectively.

spacing ratio is well defined: $r = \sum_k r_k / (N - 1)$ and

$$r_k = \frac{\min(\delta_{k+1}, \delta_k)}{\max(\delta_{k+1}, \delta_k)}, \quad \delta_k = E_{k+1} - E_k. \quad (5)$$

In the deeply localized region $R/V_0 \rightarrow 0$, $\langle r \rangle \rightarrow \langle r \rangle_{\text{Poisson}} = 2 \ln(2) - 1 \approx 0.3863$ for a Poisson distribution [72, 73], as shown in Fig 3 b). In the deep extensive region $R/V_0 \rightarrow \infty$, an asymptotic degeneracy emerges due to the periodic boundary condition and vanishing disorder. Consequently, $\langle r \rangle \rightarrow 0$ in this limit, instead of $\langle r \rangle_{\text{GOE}} \approx 0.5307$ for a Gaussian orthogonal ensemble as one might naïvely assume. As $\langle r \rangle$ also changes rapidly at $R = V_0$, this assures of a localization transition boundary as shown in Fig. 3 c).

Next, we investigate the spectra and wavefunctions at different phase regimes. As some typical examples, we show E_n and $\sqrt{|p_0^{LR}(j)|}$ in Fig. 4 for four sets of $\{t, \gamma_0\}$ marked in Fig. 1 a) : P_1 in the localized phase, P_2 in the \mathcal{PT} -symmetric and extended phase, P_3 in \mathcal{PT} -broken and extended phase, and B_{60} at the localization transition boundary. Here, $\sqrt{|p_0^{LR}(j)|}$ corresponds to the eigenstate with eigenenergy E_0 closest to 0, which is near the center of the spectrum. The numerical examples are calculated using $\varphi \approx 0.157$ and $N = 1597$. Figure 4 a) and b) shows a purely real spectrum and localized wavefunction at P_1 . At P_2 , the spectrum is also purely real as shown in Fig. 4 c), but the wavefunction spreads across all sites in Fig. 4 d). Complex conjugate pairs show up in the spectrum in Fig. 4 e), and the extensive wavefunction is shown in Fig. 4 f) for P_3 . In Fig. 4 g) and h), the spectrum and wavefunction for $R = V_0$ and $\theta = 60^\circ$

(B_{60}) are depicted. As this point is at the phase boundary between localized and extensive region, we expect the system to show critical behavior. Indeed, looking at the wavefunction we can see that it is not completely smeared over the chain. The peaks are larger and the wavefunction looks less dense as for the extended states in Fig. 4 d) and f). This is a signature of a multifractal wavefunction. To investigate the critical behavior of the system further, we employ a multifractal analysis.

Multifractal analysis.—To analyze the scaling behavior of the wavefunctions, we apply the approach detailed by Refs. [47, 68, 74] and only mention the key steps here. For a lattice with length $N = F_n$, where F_n is the n -th Fibonacci number, a scaling index α_j can be defined as

$$|p_0^{LR}(j)| = F_n^{-\alpha_j}. \quad (6)$$

For an extensive wavefunction, $\alpha_j \sim 1$ since $|p_0^{LR}(j)| \sim 1/F_n$. For a localized state, on the other hand, $|p_0^{LR}(j)|$ is nonzero only on a finite number of lattice sites. Therefore, $\alpha_j \sim 0$ on these few localized sites and $\alpha_j \rightarrow \infty$ on the other sites. For critical wavefunctions, the index α_j would distribute on a finite interval $[\alpha_{\min}, \alpha_{\max}]$. Hence, we may use α_{\min} in the thermodynamic limit $n \rightarrow \infty$ to characterize the scaling behavior: $\alpha_{\min} = 1$ for extensive states, $\alpha_{\min} = 0$ for localized states and $0 < \alpha_{\min} < 1$ for critical states. In the numerical calculations, we average α_{\min} over different quasi-disorder configurations for finite n . We fit the datapoints with a linear function to extrapolate the limit $1/n \rightarrow 0$. We present the results of the multifractal scaling in Fig. 5. In Fig. 5 a), the purple pentagons correspond to P_1 in the localized phase,

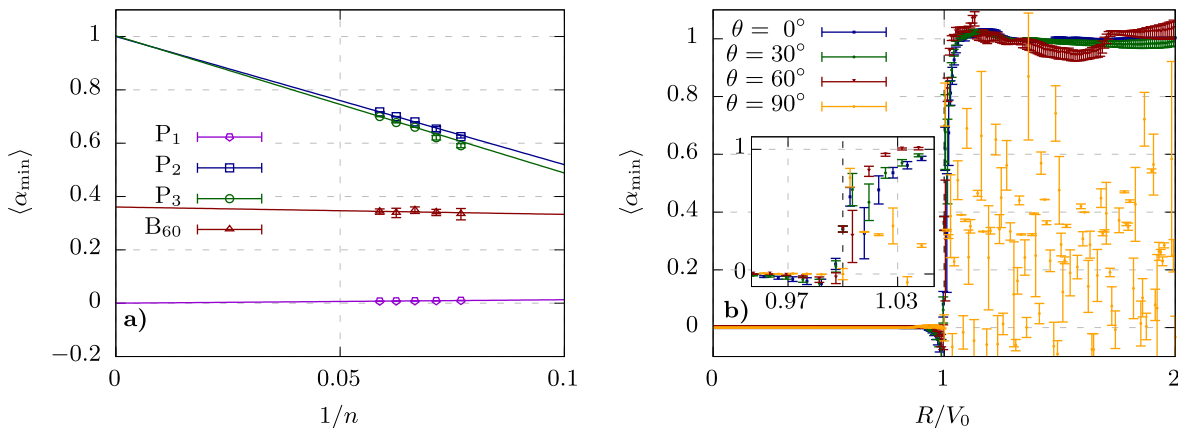


FIG. 5: a) shows $\langle \alpha_{\min} \rangle$ for different chain length $N = F_n$ with $n = 13 - 17$ for P_1 , P_2 , P_3 and B_{60} defined in Fig. 1 a). Extrapolation of $\langle \alpha_{\min} \rangle$ to $1/n \rightarrow 0$ limit can distinguish extensive, localized and critical phases. b) displays the values of $\langle \alpha_{\min} \rangle$ for $1/n \rightarrow 0$ obtained from extrapolation for different θ , illustrating the localization transition at $R = V_0$. The inset illustrate a zoom-in near $R = V_0$, emphasizing the critical index $\langle \alpha_{\min} \rangle$ all collapse approximately on 0.36 for different θ except $\theta = 90^\circ$.

where the extrapolation reveals $\langle \alpha_{\min} \rangle \rightarrow 0$. Both the blue squares and green circles that correspond to P_2 and P_3 respectively show the trend $\langle \alpha_{\min} \rangle \rightarrow 1$, confirming the wavefunctions are extensive in both phases. At the localization transition boundary B_{60} , the extrapolation of red triangles gives $\langle \alpha_{\min} \rangle \approx 0.361$, as a signature of the multifractal nature of the critical wavefunction. In Fig. 5 b) we display the extrapolated value of α_{\min} as a function of R . $\langle \alpha_{\min} \rangle$ stays at zero for the localized phase region $R < V_0$. At the boundary, the value rises quickly in the critical region until the value assumes the extended one. At the critical point $R = V_0$ the value of $\langle \alpha_{\min} \rangle \approx 0.361 \pm 0.024$ stays constant for all simulated values of θ except $\theta = 90^\circ$. The good agreement of $\langle \alpha_{\min} \rangle$ between different θ at the critical point can be observed in the inset of Fig. 5 b) where we show the zoomed region around $R = V_0$, revealing the critical region within $R \in [0.96, 1.04]$. We notice, $\theta = 90^\circ$, $R > V_0$ correspond to the “special ray” mentioned earlier, where we don’t average over φ , hence the finite-size effects become more severe. Nevertheless, despite the discontinuity and large error bars of α_{\min} on the “special ray”, the wavefunction can be classified as multifractal as $0 < \alpha_{\min} < 1$. This implies the system is critical at $t = 0$ in the \mathcal{PT} -broken phase, which will be explored in a more systematic way in future studies.

Conclusion.—We have studied a generalized \mathcal{PT} -symmetric AAH model. We have observed a \mathcal{PT} -symmetric phase $\gamma_0 < V_0$ that is robust against disorder and system size. Furthermore, we have calculated the $\langle \text{MIPR} \rangle$ and carried out the energy gap statistics to characterize the localized and extensive phases. We report a localized phase within a quarter circle $\sqrt{\gamma_0^2 + t^2} \leq V_0$. Additionally, the system features a critical behavior at the localization transition boundary $R = V_0$ and a special ray $\{R > V_0, \theta = 90^\circ\}$, where we have analyzed

fractal behaviors of the wavefunction.

Acknowledgement.—We are grateful to Brendan C. Mulkerin for fruitful discussions. This research was supported by the Australian Research Council’s (ARC) Discovery Program, Grant No. DP180102018 (X.-J.L), Grant No. DP170104008 (H.H.), and Grants No. DE180100592 and No. DP190100815 (J.W.).

Appendix A: Symmetries of the system

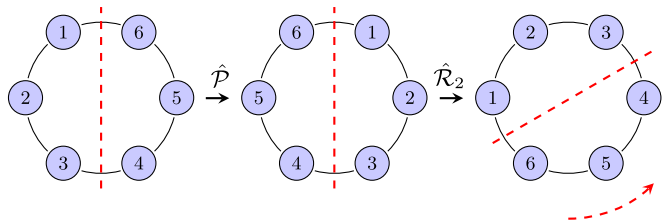


FIG. 6: An illustration of the \hat{P} and \hat{R}_k operators on a $N = 6$ lattices subject to periodic boundary condition.

\mathcal{PT} -symmetry refers to a combined parity \mathcal{P} and time-reversal \mathcal{T} symmetry. The effects of corresponding space-reflection operator \hat{P} and time-reversal operator \hat{T} on a discrete system are,

$$\hat{T}i\hat{T} = -i, \quad \hat{P}\hat{c}_j^\dagger\hat{P} = \hat{c}_{N+1-j}^\dagger. \quad (\text{A1})$$

Applying the combined $\hat{P}\hat{T}$ operator to our model Hamiltonian Eq. (1) yields

$$\hat{P}\hat{T}\hat{H}(\varphi)\hat{T}\hat{P} = \hat{H}(\bar{\varphi}), \quad (\text{A2})$$

where $\bar{\varphi} = -2\pi\beta(N+1) - \varphi \pmod{2\pi}$. We have applied $\sin(-\phi) = -\sin\phi$ and $\cos(-\phi) = \cos\phi$ in the

derivation. Here, we adopt $\beta = M/N$, where M and N are mutually prime. Therefore, one can verify that if $\varphi = \pi - \pi\beta \pmod{2\pi}$ or $2\pi - \pi\beta \pmod{2\pi}$, $\hat{\varphi} = \varphi \pmod{2\pi}$, i.e., the Hamiltonian is \mathcal{PT} -symmetric. A key feature of \mathcal{PT} -symmetric Hamiltonian is its purely real or complex-conjugate-pairs spectrum. Nevertheless, in principle, such features only requires the existence of an antiunitary operator to commute with the Hamiltonian. We can construct an antiunitary operator as $\hat{A}_k = \hat{\mathcal{R}}_k \hat{\mathcal{P}} \hat{\mathcal{T}}$, where \mathcal{R}_k is a unitary operator “rotating” the system by $k \in \mathbb{Z}$ sites in the counter-clockwise direction (see Fig. 6 for an illustrative example):

$$\mathcal{R}_k^\dagger c_j^\dagger \mathcal{R}_k = c_{j+k}^\dagger. \quad (\text{A3})$$

Applying \mathcal{R}_k on the Hamiltonian with periodic boundary conditions gives

$$\hat{\mathcal{R}}_k^\dagger \hat{H}(\varphi) \hat{\mathcal{R}}_k = \hat{H}(\varphi_k), \quad (\text{A4})$$

where $\varphi_k = \varphi - 2\pi\beta k$. Since $\hat{\mathcal{R}}_k$ is unitary, the spectra of $\hat{H}(\varphi)$ and $\hat{H}(\varphi_k)$ are the same. In addition, from the theorem of modular inverses [75], there is a solution to $Mk_1 = 1 \pmod{N}$ if and only if M and N are co-prime, which implies we can always find a $k_1 = M^{-1} \pmod{N}$ that satisfies $\varphi_{k_1} = \varphi - 2\pi/N$. Therefore, the spectrum of $\hat{H}(\varphi)$ is periodic as a function of φ with periodicity $2\pi/N$. As a result, the spectrum of $\hat{H}(\varphi)$ are always real or complex-conjugate-pairs, i.e. \mathcal{PT} -symmetric, for $\varphi = \pi - \beta\pi + 2k\pi/N \pmod{2\pi}$ or $2\pi - \beta\pi + 2k\pi/N \pmod{2\pi}$. This condition is equivalent to $\varphi = (2k+1)\pi/N \pmod{2\pi}$ for even chain and $\varphi = k\pi/N \pmod{2\pi}$ for odd chain with $k \in \mathbb{Z}$. The number of these “ \mathcal{PT} -symmetric” points of φ becomes infinite for $N \rightarrow \infty$, and the spacing between adjacent points vanishes. The periodicity of the spectrum also gives a technical benefit: we only need to average φ over $[0, 2\pi/N)$ to emulate the disorder realisation average.

Appendix B: Phase diagram for $E \approx 0$

In order to rule out the possibility of a mobility edge we simulate $\langle \text{MIPR} \rangle$ and $\langle r \rangle$. We calculate those observables for the 50 eigenstates with their real part of the energy closest to $E \approx 0$ which corresponds to the infinite temperature limit. In Fig. 7 the phase diagrams

are depicted. The $\langle \text{MIPR} \rangle$ in subfig. a) in the semicircle $R \leq V_0$ has decreased in value, but is clearly non-zero. The gap statistics in subfig. b) is indistinguishable from Fig. 1 b). We conclude that a localized region still exists at $T \rightarrow \infty$ and no trace of a mobility edge was found in the system.

Appendix C: Multifractal

For a lattice of size F_n where F_n is the n -th Fibonacci number, $p_k^{\text{LR}}(j) = |\psi_k^L(j)\psi_k^R(j)|$, $j \in [1, F_n]$ plays the role of the onsite probabilities for a given eigenstate with energy E_k . We usually select the energy E_0 closest to $E = 0$. Depending on whether the system is in an extensive phase or localized phase, the wavefunction either can be smeared over the lattice or be localized at a single site. Generally, to allow a smooth transition between the two cases we can define a scaling exponent α such that

$$p_0^{(n)}(j) = F_n^{-\alpha_j^{(n)}}. \quad (\text{C1})$$

At the localization phase transition boundary, $\alpha_j^{(n)}$ distribute between $[\alpha_{\min}^{(n)}, \alpha_{\max}^{(n)}]$. The multifractal analysis for a given level of approximation n can be extrapolated in the thermodynamic limit as $\alpha_{\min} = \lim_{n \rightarrow \infty} \alpha_{\min}^{(n)}$. Thus by identifying the minimum value α_{\min} we can classify the wavefunction as extended for $\alpha_{\min} = 1$, critical for $1 > \alpha_{\min} > 0$ and localized for $\alpha_{\min} = 0$. For the numerical calculation of α_{\min} , we follow the work by Hiramoto and Kohmoto [47, 74] who treat α_{\min} as energy of a canonical system. They then define an entropy that can be related to the onsite probabilities of the chain. The scaling exponent is given in terms of a parameter $q \in \mathbb{R}$

$$\alpha = \frac{-1}{n\epsilon} \frac{d \ln[Z_n(q)]}{dq}, \quad Z_n(q) = \sum_{j=1}^{F_n} p_j^q \quad (\text{C2})$$

where $\epsilon = \ln[(\sqrt{5}+1)/2]$ is the logarithm of the golden ratio. We vary q to find the minimum of α for chain lengths between $N = 233 - 1597$. Shorter chains were omitted as $n < 13$ was not sufficient for the scaling. For the numerical calculations we average over the quasi-disorder configurations and we fit the datapoints with a linear function to extrapolate the $1/n \rightarrow 0$ limit.

[1] V. V. Sokolov and V. G. Zelevinsky, Phys. Lett. B **202**, 10 (1988).
 [2] V. V. Sokolov and V. G. Zelevinsky, Nucl. Phys. A **504**, 562 (1989).
 [3] I. Rotter, Rep. Prog. Phys. **54**, 635 (1991).
 [4] V. V. Sokolov and V. G. Zelevinsky, Ann. Phys. (NY) **216**, 323 (1992).

[5] H. Carmichael, *An Open System Approach to Quantum Optics* (Springer, 1993).
 [6] F. M. Dittes, Phys. Rep. **339**, 215 (2000).
 [7] A. J. Daley, Adv. Phys. **63**, 77 (2014).
 [8] Y. Ashida, S. Furukawa, and M. Ueda, Phys. Rev. A **94**, 053615 (2016).

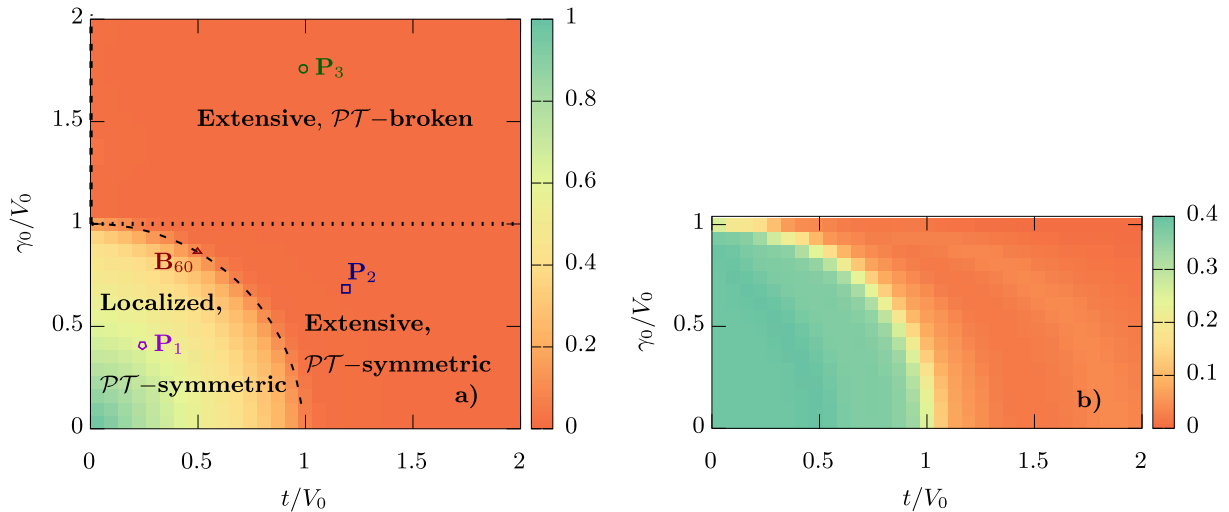


FIG. 7: Phase diagrams for the MIPR in subfig. a) and $\langle r \rangle$ ins subfig. b) of the system for $N = 233$ at infinite temperature. The MIPR in the localized region in subfig. a) has decreased but is still clearly visible. The gap statistics in subfig. b) seems to be almost indistinguishable from fig. 1. No trace of a mobility edge was found in the system.

- [9] Y. Ashida, S. Furukawa, and M. Ueda, Nat. Comm. **8**, 15791 (2017).
- [10] C. M. Bender and S. Boettcher, Phys. Rev. Lett. **80**, 5243 (1998).
- [11] C. M. Bender, S. Boettcher, and P. N. Meisinger, J. Math. Phys. (NY) **40**, 2201 (1999).
- [12] C. M. Bender, D. C. Brody, and H. F. Jones, Phys. Rev. Lett. **89**, 270401 (2002).
- [13] C. M. Bender, S. Boettcher, and P. N. Meisinger, Rep. Prog. Phys. **70**, 947 (2007).
- [14] C. M. Bender, D. C. Brody, and M. P. Müller, Phys. Rev. Lett. **118**, 130201 (2017).
- [15] O. Bendix, R. Fleischmann, T. Kottos, and B. Shapiro, Phys. Rev. Lett. **103**, 030402 (2009).
- [16] R. El-Ganainy, K. G. Makris, D. N. Christodoulides, and Z. H. Musslimani, Opt. Lett. **32**, 2632 (2007).
- [17] K. G. Makris, R. El-Ganainy, D. N. Christodoulides, and Z. H. Musslimani, Phys. Rev. Lett. **100**, 103904 (2008).
- [18] Z. H. Musslimani, K. G. Makris, R. El-Ganainy, and D. N. Christodoulides, Phys. Rev. Lett. **100**, 030402 (2008).
- [19] S. Longhi, Phys. Rev. Lett. **103**, 123601 (2009).
- [20] S. Longhi, Phys. Rev. B **80**, 235102 (2009).
- [21] A. Guo, G. J. Salamo, D. Duchesne, R. Morandotti, M. Volatier-Ravat, V. Aimez, G. A. Siviloglou, and D. N. Christodoulides, Phys. Rev. Lett. **103**, 093902 (2009).
- [22] C. E. Rüter, K. G. Makris, R. El-Ganainy, D. N. Christodoulides, M. Segev, and D. Kip, Nat. Phys. **6**, 192 (2010).
- [23] A. Regensburger, C. Bersch, M.-A. Miri, G. Onishchukov, D. N. Christodoulides, and U. Peschel, Nature **488**, 167 (2012).
- [24] B. Peng, Ş. K. Özdemir, F. Lei, F. Monifi, M. Gianfreda, G. L. Long, S. Fan, F. Nori, C. M. Bender, and L. Yang, Nature **10**, 394 (2014).
- [25] L. Feng, Z. J. Wong, R.-M. Ma, Y. Wang, and X. Zhang, Science **346**, 972 (2014).
- [26] H. Hodaei, M.-A. Miri, M. Heinrich, D. N. Christodoulides, and M. Khajavikhan, Science **346**, 975 (2014).
- [27] B. Zhen, C. W. Hsu, Y. Igarashi, L. Lu, I. Kaminer, A. Pick, S.-L. Chua, J. D. Joannopoulos, and M. Soljčić, Science **525**, 354 (2015).
- [28] J. M. Zeuner, M. C. Rechtsman, Y. Plotnik, Y. Lumer, S. Nolte, M. S. Rudner, M. Segev, and A. Szameit, Phys. Rev. Lett. **115**, 040402 (2015).
- [29] C. Poli, M. Bellec, U. Kuhl, F. Mortessagne, and H. Schomerus, Nat. Comm. **6**, 6710 (2015).
- [30] J. Doppler, A. A. Mailybaev, J. Böhm, U. Kuhl, A. Girschik, F. Libisch, T. J. Milburn, P. Rabl, N. Moiseyev, and S. Rotter, Nature **537**, 76 (2016).
- [31] C. M. Bender, B. K. Berntson, D. Parker, and E. Samuel, Am. J. Phys. **81**, 173 (2013).
- [32] J. Li, A. K. Harter, J. Liu, L. de Melo, Y. N. Joglekar, and L. Luo, Nat. Comm. **10**, 855 (2019).
- [33] L. Dal Negro, C. J. Oton, Z. Gaburro, L. Pavesi, P. Johnson, A. Lagendijk, R. Righini, M. Colocci, and D. S. Wiersma, Phys. Rev. Lett. **90**, 055501 (2003).
- [34] Y. Lahini, R. Pugatch, F. Pozzi, M. Sorel, R. Morandotti, N. Davidson, and Y. Silberberg, Phys. Rev. Lett. **103**, 013901 (2009).
- [35] Y. E. Kraus, Y. Lahini, Z. Ringel, M. Verbin, and O. Zilberberg, Phys. Rev. Lett. **109**, 106402 (2012).
- [36] M. Verbin, O. Zilberberg, Y. E. Kraus, Y. Lahini, and Y. Silberberg, Phys. Rev. Lett. **110**, 076403 (2013).
- [37] M. Verbin, O. Zilberberg, Y. Lahini, Y. E. Kraus, and Y. Silberberg, Phys. Rev. B **91**, 064201 (2015).
- [38] G. Roati, C. D'Errico, L. Fallani, M. Fattori, C. Fort, M. Zaccanti, G. Modugno, M. Modugno, and M. Inguscio, Nature **453**, 895 (2008).
- [39] G. Modugno, Rep. Prog. Phys. **73**, 102401 (2010).
- [40] P. W. Anderson, Phys. Rev. **109**, 1492 (1958).
- [41] S. Aubry and G. André, Ann. Isr. Phys. Soc. **3**, 18 (1980).
- [42] J. Biddle and S. Das Sarma, Phys. Rev. Lett. **104**, 070601 (2010).
- [43] X. Cai, L.-J. Lang, S. Chen, and Y. Wang, Phys. Rev. Lett. **110**, 176403 (2013).

- [44] W. DeGottardi, D. Sen, and S. Vishveshwara, *Phys. Rev. Lett.* **110**, 146404 (2013).
- [45] S. Ganeshan, J. H. Pixley, and S. Das Sarma, *Phys. Rev. Lett.* **114**, 146601 (2015).
- [46] F. Liu, S. Ghosh, and Y. D. Chong, *Phys. Rev. B* **91**, 014108 (2015).
- [47] J. Wang, X.-J. Liu, G. Xianlong, and H. Hu, *Phys. Rev. B* **93**, 104504 (2016).
- [48] Y. Cao, X. Gao, X.-J. Liu, and H. Hu, *Phys. Rev. A* **93**, 043621 (2016).
- [49] J. C. C. Cestari, A. Foerster, and M. A. Gusmão, *Phys. Rev. B* **93**, 205441 (2016).
- [50] Q.-B. Zeng, S. Chen, and R. Lü, *Phys. Rev. B* **94**, 125408 (2016).
- [51] X.-D. Bai, J. Wang, X.-J. Liu, J. Xiong, F.-G. Deng, and H. Hu, *Phys. Rev. A* **98**, 023627 (2018).
- [52] Q.-B. Zeng, S. Chen, and R. Lü, *Phys. Rev. A* **95**, 062118 (2017).
- [53] T. Liu, H. Guo, Y. Pu, and S. Longhi, *Phys. Rev. B* **102**, 024205 (2020).
- [54] Q.-B. Zeng, Y.-B. Yang, and Y. Xu, *Phys. Rev. B* **101**, 020201 (2020).
- [55] N. Hatano and D. R. Nelson, *Phys. Rev. Lett.* **77**, 570 (1996).
- [56] N. Hatano and D. R. Nelson, *Phys. Rev. B* **56**, 8651 (1997).
- [57] N. Hatano and D. R. Nelson, *Phys. Rev. B* **58**, 8384 (1998).
- [58] R. Hamazaki, K. Kawabata, and M. Ueda, *Phys. Rev. Lett.* **123**, 090603 (2019).
- [59] Z. Gong, Y. Ashida, K. Kawabata, K. Takasan, S. Higashikawa, and M. Ueda, *Phys. Rev. X* **8**, 031079 (2018).
- [60] C. Mejía-Cortés and M. I. Molina, *Phys. Rev. A* **91**, 033815 (2015).
- [61] D. M. Jović, C. Denz, and M. R. Belić, *Opt. Lett.* **37**, 4455 (2012).
- [62] Y. N. Joglekar, D. Scott, M. Babbey, and A. Saxena, *Phys. Rev. A* **82**, 030103 (2010).
- [63] C. H. Liang, D. D. Scott, and Y. N. Joglekar, *Phys. Rev. A* **89**, 030102 (2014).
- [64] C. Yuce, *Phys. Lett. A* **378**, 2024 (2015).
- [65] Y. N. Joglekar and A. Saxena, *Phys. Rev. A* **83**, 050101 (2011).
- [66] D. D. Scott and Y. N. Joglekar, *Phys. Rev. A* **83**, 050102 (2011).
- [67] A. K. Harter, T. E. Lee, and Y. N. Joglekar, *Phys. Rev. A* **93**, 062101 (2016).
- [68] See Appendix for the details of (A) analytical investigation of the system's symmetry, (B) $\langle \text{MIPR} \rangle$ and $\langle r \rangle$ near the center of the spectrum, and (C) technical details of our multifractal analysis.
- [69] C. M. Bender and S. Boettcher, *Physical Review Letters* **80**, 5243 (1998).
- [70] L. Schäfer and F. Wegner, *Zeitschrift für Physik B Condensed Matter* **39**, 281 (1980).
- [71] G. H. Zhang and D. R. Nelson, *Physical Review E* **100** (2019).
- [72] V. Oganesyan and D. A. Huse, *Physical Review B* **75** (2007).
- [73] A. Pal and D. A. Huse, *Physical Review B* **82** (2010).
- [74] H. Hiramoto and M. Kohmoto, *Physical Review B* **40**, 8225 (1989).
- [75] K. H. Rosen, *Elementary Number Theory and Its Applications* (Pearson/Addison Wesley, 2005).